

AD-A060 113

CHICAGO UNIV ILL JAMES FRANCK INST
MEASUREMENT OF FAST DESORPTION KINETICS OF D2 FROM TUNGSTEN BY --ETC(U)
MAR 78 J P COWIN, D J AUERBACH, C BECKER

F/G 7/4

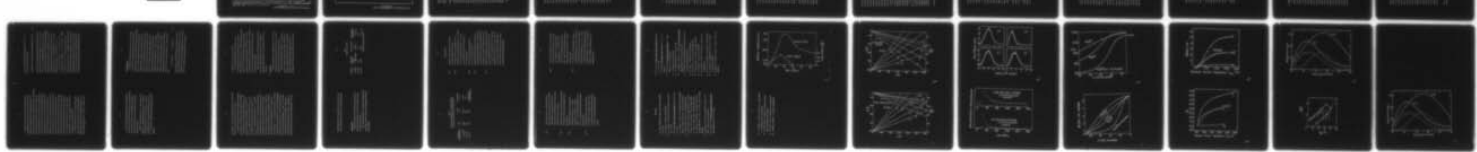
N00014-77-C-0240

NL

UNCLASSIFIED

| OF |
AD
AD 60113

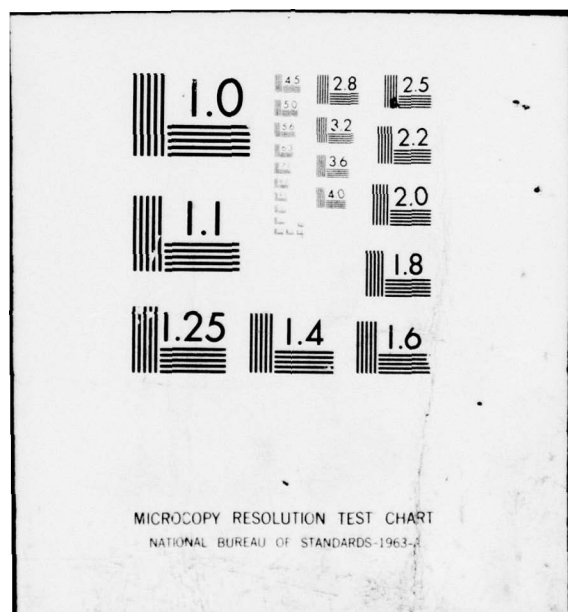
EFF FILE



END

DATE
FILMED
12-78

DDC



MICROCOPY RESOLUTION TEST CHART
NATIONAL BUREAU OF STANDARDS-1963-2

Unclassified

SECURITY CLASSIFICATION OF THIS PAGE (When Data Entered)

REPORT DOCUMENTATION PAGE			READ INSTRUCTIONS BEFORE COMPLETING FORM
1. REPORT NUMBER	2. GOVT ACCESSION NO.	3. RECIPIENT'S CATALOG NUMBER	
4. TITLE (and Subtitle) MEASUREMENT OF FAST DESORPTION KINETICS OF D ₂ FROM TUNGSTEN BY LASER INDUCED THERMAL DESORPTION.		5. TYPE OF REPORT & PERIOD COVERED Journal Article	
7. AUTHOR(s) J. P. Cowin, D. J. Auerbach*, C. Becker and L. Wharton *Dept. of Chem., Johns Hopkins U., Baltimore, MD		6. PERFORMING ORG. REPORT NUMBER AFOSR-77-3186	
9. PERFORMING ORGANIZATION NAME AND ADDRESS The University of Chicago 5801 S. Ellis Ave. Chicago, IL 60637		8. CONTRACT OR GRANT NUMBER(s) ONR N00014-77-C-0240	
11. CONTROLLING OFFICE NAME AND ADDRESS Office of Naval Research Physics Program Office Arlington, VA 22217		10. PROGRAM ELEMENT, PROJECT, TASK AREA & WORK UNIT NUMBERS VAFOSR-77-3186	
14. MONITORING AGENCY NAME & ADDRESS (if different from Controlling Office) 12 26p.		12. REPORT DATE March, 1978	
		13. NUMBER OF PAGES 44	
		15. SECURITY CLASS. (of this report) Unclassified	
		15a. DECLASSIFICATION/DOWNGRADING SCHEDULE DDC OCT 20 1978 PUBLISHED F	
16. DISTRIBUTION STATEMENT (of this Report) Approved for public release; distribution unlimited 10 James P. Cowin, Daniel J. Auerbach, Charles Becker, Lennard Wharton			
17. DISTRIBUTION STATEMENT (of the abstract entered in Block 20, if different from Report) 11			
18. SUPPLEMENTARY NOTES Accepted for publication in Surface Science			
19. KEY WORDS (Continue on reverse side if necessary and identify by block number) Desorption D ₂ Kinetics W Thermal Desorption Laser Thermal Desorption			
20. ABSTRACT (Continue on reverse side if necessary and identify by block number) The laser desorption method has been shown analogous to the fast temperature jump method used for studying reactions in condensed phases, and is capable of sorting out elementary processes that have differing activation energies. The variation of total flux desorbed vs. maximum temperature reached and vs. initial surface coverage determined, gave with the aid of a model kinetic rate expression desorption rate parameters. It was shown that at rates 105 times faster than previous measurements the kinetics of desorption of hydrogen follows the same reaction equations. Since the desorption time is short compared to the (cont'd. on reverse)			

DD FORM 1473 EDITION OF 1 NOV 65 IS OBSOLETE
JAN 73

Unclassified 403-024
SECURITY CLASSIFICATION OF THIS PAGE (When Data Entered)

Unclassified

SECURITY CLASSIFICATION OF THIS PAGE(When Data Entered)

20. Abstract (cont'd.)

range of desorbate flight times to the mass spectrometer detector, velocity distributions of the desorbing species were determined. This along with the surface temperature history gave additional information on the reaction rate model. In the present experiments a significant number of desorbate-desorbate collisions could occur. Corrections were made for the collisional effects in the interpretation of the data. In addition it was shown how modifications of the technique could be used to mitigate the effects of collisions.

ACCESSION for	
NTIS	White Section <input checked="" type="checkbox"/>
DDC	Buff Section <input type="checkbox"/>
UNANNOUNCED <input type="checkbox"/>	
JUSTIFICATION	
BY	
DISTRIBUTION/MATERIALITY CODES	
S. CHAL	
A	

Unclassified

SECURITY CLASSIFICATION OF THIS PAGE(When Data Entered)

J. P. Cowin, D. J. Auerbach*, C. Becker, and L. Wharton
The James Franck Institute and The Department of Chemistry
The University of Chicago, Chicago, Illinois 60637

Abstract

A laser heating technique for studying fast surface processes has been applied in an initial study to the thermal desorption of D₂ from a polycrystalline tungsten sample. This technique is a means for measuring surface reactions at rates, concentrations, and temperatures that approach conditions of technical interest, but with the high degree of definition and control made possible with an ultrahigh vacuum apparatus. The method is analogous to the fast temperature jump method used for studying reactions in condensed phases, and can sort out elementary processes that have differing activation energies. The variation of total flux desorbed with maximum surface temperature reached and initial surface coverage serves, with the aid of a model kinetic rate expression, to determine the desorption rate parameters. It is shown that the desorption of D₂ from W at rates of 5×10^7 monolayers/sec is governed by the same kinetics as obtained by extrapolating previous measurements made at a rate about 10^5 times slower. The surface is subjected to a sufficiently fast and large temperature rise to desorb surface atoms or molecules in a time short compared to the range of flight times to a mass spectrometer detector. In this way the velocity distribution of the desorbing species may be determined. This along with the surface temperature time history gives additional information on the reaction rate model and also whether the species are emerging in translational thermal equilibrium with the surface. In the present experiments a significant number of desorbate-desorbate collisions occur. Corrections are made for the collision effects in the interpretation of the data. It is shown how modifications of the technique can be made to substantially eliminate these effects. The present conditions were laser pulse width of 3×10^{-8} sec and surface temperature rise of 300 to 3000 K.

I. Introduction

The ability to bring a variety of techniques together to bear upon a problem has been particularly important in surface science. We are beginning

a series of experiments utilizing a very fast laser heating technique to obtain

new information on adsorbate systems. We chose for study the D₂/W system for several reasons: It is a prime example of an atom-recombination description. The system is relatively simple and easy to study; much previous data is available for comparison. The binding energy is high enough for room temperature adsorption, and low enough to allow laser desorption without surface melting or plasma. Finally, D₂ has a lower background level in our detector than does H₂.

Fundamental questions have existed about the validity of extrapolating molecular beam measurements of surface reaction rates to much higher temperatures and pressures. (1) The prime motivation of this work is to provide a means for measuring surface reactions in a UHV apparatus at rates, surface concentrations, and temperatures that approach conditions of technical interest. An important feature of this technique is that it permits determination of the velocity distributions of the desorbing molecules. This gives insight into the desorption dynamics, for example, whether there is translational energy equilibration with the surface. If a desorbed reaction product has a distinctive velocity distribution, or angular distribution, this chemical "fingerprint" could allow one to determine if a different reaction with the same product had the same final step. The vast range of heating rates potentially available with the present technique, 10^5 to 10^{11} °K/sec, can test kinetic

*Present address: IBM Research Laboratories, 5600 Cottle Road, San Jose, CA 95193

mechanisms over a wide dynamic range. For the model system we studied--
 recombinative desorption of D_2 and H_2 from polycrystalline W--we have
 shown that the kinetic parameters are about the same at 10^{11} °K/sec and 1300 K
 as those determined at 10^3 °K/sec and 700 K. (2) The large dynamic range
 available should clarify multistep reactions as the relative rates of the
 elementary steps may be significantly changed. Diffusion distances are
 reduced because of the lower activation energy of diffusion compared to other
 competing processes such as, for example, desorption. This may allow
 minimization or control of the role that scarce, very active sites play in
 surface reactions. It may also be possible to desorb chemical intermediates
 otherwise not seen. Combinations of reactants may be brought together at
 high concentrations that are unachievable at lower heating rates.

Other advantages are purely technical. No internal chopper is needed
 for velocity measurements. The specimen need not have electrical leads or
 special shapes. There are no interferences from reactions on other surfaces
 of the specimen than the one under study. Some insulators could be heated,
 as well as thin films. Since for metals only a 10^{-2} to 10^{-4} cm deep layer
 is heated, cooling is very fast, allowing high repetition rates even on cryogenic
 surfaces. Molten surfaces can be produced and would be self-supported.

One striking advantage is the high signal to noise at the present high angular
 resolution: For a desorbed monolayer reaching a detector over a time of
 10^{-4} to 10^{-3} seconds, a single desorption suffices to give excellent signal
 to noise with 1 μsec channel widths.

Previous uses of laser heating in surface science have been relatively few.

Considerable work has been published relating to laser vaporization for analytical purposes⁽³⁾ or laser fusion reactors. Some interesting studies of vaporizing solids have been conducted. (4, 5) Desorption of neutral adsorbates has been studied in relation to production of clean surfaces, (6) thermal desorption^(4, 7) and photodesorption. (8) Velocity distributions for laser desorbed neutral adsorbates are almost non-existent. (4)

II. Theory: Laser Heating

An excellent treatment of many aspects of laser heating of solids has been given by Ready. (4) The light is adsorbed by interaction with the conduction electrons in the metal. Since the time for electronic relaxation and transfer of the energy to the lattice phonons, $\sim 10^{-13}$ sec, (9) is much shorter than the minimum characteristic heating time used in our experiments, 10^{-8} seconds, the ordinary bulk thermal transfer laws are adequate. The absorption of the light does not take place at the surface of the metal, but extends inward a characteristic "skin depth" of several hundred Å, due to the optical properties of the metal^(10, 11) and the mean free path of the electrons. (9) However, this is much shorter than the depth to which the heat travels by conduction, $(\Delta t \kappa/c)^{1/2}$, with Δt being the heating duration, κ the thermal conductivity, and c the heat capacity. For W with $\Delta t = 10^{-8}$ sec, $\kappa = 1.21$ W/cm/°K,
 $c = 2.9 \text{ J/cm}^3/\text{°K}$, this distance is 6500 Å. Reradiation by the surface during heating is negligible. Thus the heating is adequately described by a heat source at the mathematical surface of a semi-infinite solid W mass. If κ , c , and the optical absorptivity ϵ are assumed independent of temperature, the surface temperature produced by an incident light flux $R(t)$, beginning at time $t=0$, can be readily shown to be⁽⁴⁾,

Thermal Desorption

$$T(t) = \epsilon / (\kappa c m)^{1/2} \int_0^t R(r-t') / r^{1/2} dr + T(0) . \quad (1)$$

Figure (1) shows the predicted $T(t)$ for a triangular $R(t)$ with FWHM of 30 nsec and average power of 2.5×10^7 watts/cm², $\epsilon = .37$, and the thermal properties of W at 1000K. (10,12) This corresponds in this experiment roughly to the conditions for the data in Figs. (6) and (7). Because the variation of $\epsilon / (\kappa c)^{1/2}$ from that at 1000K is less than 8% over the range 300 to 2000K, assuming it to be constant is a reasonable approximation. The temperature profile of Fig. (1), rescaled for different laser power, was used in all desorption calculations. The temperature prediction scaling factors were obtained by direct calibration, as discussed in the next section.

At very high irradiances plasma formed. We observed a sharp threshold for plasma formation, characterized by high energy ion production, at an average laser power of 5×10^7 w/cm². The plasma is believed to originate in the swarm of desorbed molecules above the surface and has a sharp threshold due to an exponential production of charged particles by the "inverse bremsstrahlung" mechanism. The plasma formation is triggered by electrons resulting from multiphoton ionization or by thermionic electrons from the tungsten or its alkali metal impurities. (4) The desorption results reported here were obtained below the plasma threshold.

The value of fast thermal desorption is obvious where peculiarities in the resultant velocity distributions give direct insight into the desorption dynamics. However, when studying kinetic rates, the most appropriate information is the desorption rate as a function of surface coverage and temperature, information not obviously available from laser heating. We shall describe how this information is obtainable, and how the large heating rate range of laser desorption affects thermal desorption. Though the theory of thermal desorption has been well covered in the literature, we first reiterate some of the results which show the utility of laser desorption and aid understanding of our data.

With thermal desorption there are two operational regimes: 1) the temperature rises continuously through the (complete) desorption--the "linear heating" regime; 2) the desorption (often incomplete) takes place only near the highest temperature reached--the "isothermal" regime. For real experiments the actual temperature is seldom actually linear in time, but comparison of the results for linear and hyperbolic heating by Redhead (13) shows that desorption behavior is largely insensitive to the precise heating schedule, and depends primarily on the heating rate dT/dt ($\equiv B$) at the maximum desorption rate. The simplest desorption kinetics are often analyzed according to

$$-d\sigma / dt = v_n \sigma^n \exp(-E/kT) \quad (2)$$

where σ is the surface concentration, n the desorption order, v_n the pre-exponential, and E the desorption activation energy. This expression was numerically integrated using linear temperature time variation to obtain the temperature

of peak desorption rate, \bar{T}_p , and the temperature FWHM of the desorption process $\Delta T_{\frac{1}{2}}$. Results for the first and second order rates appear in Figs. (2) and (3) respectively. Heating rates were used which spanned the range of most conventional flash desorption, $10^0 - 10^3 \text{ K/sec}$, and the range of laser flash desorption, $10^6 - 10^{11} \text{ K/sec}$. γ was chosen as $10^{13}/\text{sec}$, $\gamma_2 \approx 10^{-3} \text{ cm}^2/\text{sec} \times 10^{15} / \text{cm}^2$, but since these are always divided by B in the calculations, other choices can be obtained by rescaling the graphs.

Clearly Redhead's rule of the near linear dependence of E on T_p is followed even at the highest heating rates, with the slope varying with the heating rate. $\Delta T_{\frac{1}{2}}$ also is seen to be nearly linear in T_p , about 1 to .3 of T_p . Not shown are calculations for coverage dependent E . The most significant effect of coverage or site dependent E is to increase $\Delta T_{\frac{1}{2}}$. For large variations of E , $\Delta T_{\frac{1}{2}}/T_p$ will approach the relative range of E about the mean. (14)

Desorption in the isothermal regime is trivial to analyze, and is conveniently described in a discussion of the general expectations of a desorption experiment. Suppose one does a series of desorption experiments where the intensity of laser heating is increased sequentially, producing increasingly higher maximum surface temperature, T_{\max} . One can readily measure the total desorbed flux, denoted $F(T_{\max})$, and, assuming Boltzmann velocity distributions, the average desorption temperature $\bar{T}(T_{\max})$ ($\approx T_p(T_{\max})$ discussed in the previous paragraph). At the lowest T_{\max} the desorbed flux F will be but a small fraction of the initial coverage,

and should vary approximately as $\exp(-E/kT_{\max})$. Since the desorption at low laser heating takes place only near T_{\max} , T_p will be nearly equal to T_{\max} . At increasing T_{\max} , F will begin to increase more slowly as a large fraction of the initial coverage is desorbed, eventually becoming constant when all is desorbed. T_p will begin to increase more slowly than T_{\max} as the latter increases, until at high T_{\max} , T_p will depend on the rate of temperature rise, i.e. approximately logarithmically on T_{\max} .

A total dynamic range of up to 10^{11} for conventional and laser desorption together greatly extends the possibilities for precise and detailed kinetic analysis. As a simple example, to merely determine γ of equation 2 accurately, Redhead (13) suggests that the heating rate B be varied by at least a factor of 100. This is often extremely difficult to achieve in conventional thermal desorption because of problems of signal to noise, contamination, etc., but is readily possible with laser heating. More profound advantages are clear where multiple steps occur in a reaction or desorption. The relative importance of the steps can be significantly altered if T_p can be sufficiently changed. Referring again to Figs. (2) and (3), the addition of laser heating to conventional methods greatly increases for a given E the range of T_p accessible. Only 20 to 30% variations of T_p are possible in conventional techniques. With laser heating rates between 10^6 to 10^{11} K/sec , an increase of T_p by about 100%, is achieved, and over the total range of 10^0 to 10^{11} K/sec , T_p increases by up to 300%.

The first step in obtaining $d\sigma(T)/dt$ versus coverage, from the described flux $F(T_{\max})$ and the measured velocity distributions, is to accurately determine the surface temperature versus time. The short time scale of laser heating, 10^{-3} to 10^{-9} sec ,

prevents the use of most common techniques for measurement of the time variation of the surface temperature. The surface temperature vs. time can be determined by two complimentary methods: (1) The theory of laser heating together with an accurate measurement of the laser irradiance can be used to estimate $T(h)$. (2) The maximum surface temperature reached can be determined in the isothermal desorption limit from the measured velocity distribution, provided the molecules desorb in thermal equilibrium with the surface. Method (1) depends upon the accuracy of the measured thermal and optical parameters. The optical adsorptivity is least certain.

Method (2) depends upon the assumption of thermal equilibration. It gives T_{max} , which is used to scale the laser heating theory's $T(h)$. The two methods for determining

T_{max} agreed within 4%, as is discussed below.

Accurate kinetic rate determination uses the variation of desorbed flux $F(T_{max})$ with initial coverage and heating schedule. Computer simulation of the desorption, using the previously determined $T(h)$, is conveniently used to determine the parameters of a model kinetic equation. To illustrate that the information content of the data is comparable to that from conventional flash desorption (with the additional advantage of a greatly extended dynamic range), we point out that, roughly, for the range of T_{max} for which F is still rapidly increasing, $F(T_{max})/(\text{approximate laser pulse width})$ is about equal to the desorption rate at $T_{max} = d(T_{max})/dt$.

The above analysis does not require that the molecules desorb Boltzmann

like. If it is true that there is an equilibrium Boltzmann velocity distribution, then one can obtain the average temperatures of desorption. These can be used to help analyze the kinetics. The effect of the range $\Delta T_{\frac{1}{2}}$ of temperatures for which desorption occurs is masked by the large natural width of a Boltzmann velocity distribution. This is obviously the case in the limit of isothermal desorption. In the linear heating regime, where $\Delta T_{\frac{1}{2}}/T_p$ is not negligible, the effect on the velocity distributions is small: the increase in width of a Boltzmann distribution due to the range $\Delta T_{\frac{1}{2}}$ of desorption temperatures around T_p is roughly

$$(1 + .2\Delta T_{\frac{1}{2}}/T_p)^2 \approx 1 \quad (3)$$

Even for $\Delta T_{\frac{1}{2}}/T_p = \frac{1}{2}$, the increase in velocity spread is only 2%.

III. Experimental

A polycrystalline W ribbon was exposed to a constant ambient pressure of D_2 or H_2 while heated at 20 sec intervals with a Q-switched laser. The signal arising from pulses of desorbed gas was detected by a differentially pumped mass spectrometer, and data were stored by a synchronized high speed signal averager, typically into 2 microsecond channels. For good signal to noise, 10 to 50 pulses were digitally averaged.

The W was cut from a 99.98% foil and installed without polishing.

It was initially cleaned by ohmic heating in oxygen. Auger spectra indicated that subsequent 1 sec high temperature ohmic heating flashes produced a clean surface. Before each group of 10 to 50 desorptions, the W was flashed clean and allowed to cool 100 sec (while still laser irradiated) to an estimated 380 K before data collection began. After the experiment, electron microscopic examination showed the W had a grain size of about .01 cm. Grain boundary etching was observed on the laser-irradiated surface, but there was no evidence of surface melting.

The UHV system had a working base pressure of 1×10^{-10} torr. The detector was a quadrupole mass spectrometer and was doubly differentially pumped. It had an electron bombardment ionizer 14.5 cm from the surface, an angular resolution of 1° , and could be rotated about the W surface.

The W was dosed with D_2 or H_2 by bleeding the gas into the vacuum system while monitoring with a Bayard-Albert gauge (BAG 2). The 400 l/sec ion pump was left on to limit build-up of contaminants. (15) At

higher D₂ pressures, there was a noticeable "poisoning," that is, progressive decline in signal in a series of runs by an adsorbate not desorbed by the laser heating. This decline was usually negligible over a series of fifty 20 second laser desorptions (in a small fraction of the data corrections to the measured flux were appropriately made).

Laser heating was done by imaging an aperture illuminated by a 1000 nm Q-switched Korad Nd glass laser onto the W through a glass viewport. The laser pulse had a FWHM of about 30 nsec and was nearly symmetrical. Variation of laser power at the W surface was accomplished primarily with optical filters, leaving the shape of the laser pulse unchanged. The regular firing of the laser resulted in less than 2% variation in pulse energy over 50 shots. Spatial homogeneity of the laser beam was probably not better than $\pm 25\%$, typical for this type of laser, (16) and the distribution changed from day to day, being very sensitive to mirror alignment. The laser beam struck the W at a 40° angle from the normal over an ellipse 18×24 cm.

The time integrated laser power was monitored with a beamsplitter and silicon photodiode, calibrated with a ballistic thermopile. The laser irradiance in terms of average power/cm², assuming a triangular 30 nsec FWHM laser pulse, ranged from $5 \times 10^6 \times 10^6$ w/cm².

T_{\max} and the variation of temperature with time due to the laser pulse were determined by two methods that agreed reasonably well. The first method used the calculation illustrated in Figure 1 with the optical and thermal properties of W at 1000 K. The second method used a numerical desorption simulation

with Hickmott's (2) kinetics for conditions of the lowest initial coverage data of Table 2. Here the functional form of T(t) from Figure 1 is retained, but the scale is adjusted so as to achieve agreement between the predicted T_p and that measured in Table 2 ($T_p \sim \bar{T} = 1700$ K). Being nearly in the isothermal desorption regime, the results are rather insensitive to the desorption model used. Comparing the two methods we find that a \bar{T}_{\max} of 1848 K was predicted by the first, and 1790 K by the desorption simulation method. The two values are within experimental uncertainty of each other. The use of $\bar{T} = 1700$ from Table 2 presupposes that the molecules initially desorb with thermal equilibrium velocity distributions, before gas phase collisions occur (see below). We have arbitrarily chosen the desorption simulation calibration, rescaling the calculated T(t) of figure 1 downward 3.8%, for our reported values of T_{\max} . The arbitrariness is clearly not serious.

Surface Coverage Determination

The surface coverage reached in the 20 seconds between laser desorptions should be calculable from the pressure P , the variation of the sticking coefficient S with coverage σ_f and the coverage σ_r remaining from the previous laser desorption. $S(\sigma)$ typically has been found to vary roughly as $S_0(1-\sigma/\sigma_{\max})^2$ for this system. At a constant impingement rate of Q integration gives

$$\sigma = \frac{\sigma_{\max} \sinh(f\Delta t) + \sigma_r \cosh(f\Delta t)}{\sigma_{\max} \cosh(f\Delta t) + \sigma_r \sinh(f\Delta t)} \quad \text{for } f = \frac{Q S_0}{\sigma_{\max}} \quad (4)$$

σ_{\max} at room temperature for polycrystalline W usually has been measured to be close to 10^{15} atoms/cm². The relative reproducibility of the measured value of σ_{\max} may be due to the fact that the saturation coverage of W (100) and (110) are both within 40% that of polycrystalline W (117), reducing the sensitivity to the particular microfacet structure. S_o has been measured on polycrystalline W as .3 (18), .08 (19), .14 - .18 (20), and .07 (17). The large variation may be due to the large variation of S_o for specific W planes (17). S_o has been found to be identical for both D₂ and H₂ on polycrystalline W (21) (similarly on W (110), but not on W (100) (22, 23)).

It is convenient to use 9×10^{14} atoms/cm² for σ_{\max} , that predicted by Hickmott for similar conditions (2). Using an average $S_o = .15$ and a relative BAG sensitivity for D₂ of .4, one calculates that a 20 second dose at 7.5×10^{-8} torr D₂ corresponds to an exposure $.48 \sigma_{\max} / S_o$. Our own data, however, strongly suggests that for this exposure a coverage of .8 to .9 σ_{\max} is reached,

implying the exposure is 1.1 to 1.5 σ_{\max} / S_o . The cause of the discrepancy must lie in errors in P, S_o , or σ_{\max} . Though not calibrated by us, the sensitivity of the BAG is unlikely to vary more than 25% from the manufacturer's specifications (15). S_o may be larger due to our particular microfacet composition, or the laser annealing of the surface. σ_{\max} could have been significantly reduced by competing adsorbates if they either adsorbed very quickly or were not removed by the high temperature flash. The poisoning mentioned earlier appears from Auger data to be due to CO buildup. However the

rate is much too slow to be of significance, and the CO is clearly removed by the cleaning flash. There was no Auger evidence for any other contaminants, including oxygen or carbon. Most likely errors in S_o and P both contribute to the apparent discrepancy.

To estimate surface coverage, σ_{\max} was assumed to be 9×10^{14} atoms/cm². 20 seconds at 7.5×10^{-8} torr (nominal) D₂ was assigned an exposure of

1.1 σ_{\max} / S_o , and S(σ) was as given above. At the various D₂ exposures used, the coverage calculated at the beginning of the laser desorption is given in Table 1, including the correction for the residual D₂ from the previous desorption calculated with Hickmott's kinetics, and taking T_{max} = 1830 K.

IV. Results

A large number of D₂ and H₂ desorption time of flight distributions were obtained; two representative examples appear in Fig. (4). We also observed under some circumstances H atom desorption from the surface on the order of 1% of the H₂ flux (distinct from the "cracking pattern" of H₂ in the detector). The data were transformed point by point to velocity distributions of the desorbing flux, using the appropriate Jacobian, and were least squares fitted to thermal distributions. Systematic deviations of the fitted from experimental curves were observed, particularly for large fractions of a monolayer

desorbed. Figure (5a, b) shows the systematic deviations at their largest, the 0° experimental velocity distributions being narrower, and the 60° data wider, than their respective fitted thermal distributions. These deviations are moderate in Fig. (5a, b) and are small for submonolayer desorption (Fig. 5c, d). Thus we felt it to be a reasonable simplification to use the temperatures so fitted, and number desorbed [flux] as the basis for discussion and analysis within this paper.

Corrections have been made for velocity sensitivity of the detector and the ion flight time through the quadrupole. Laser pulse width and ionizer length affected the signal negligibly. Time resolution inadvertently was limited by the preamplifier used. A first order correction for its response was made by attributing a 4.4 microsecond delay to it. Its systematic second order convolution effects, most important for the fastest desorbing molecules, were estimated to be perhaps 6% on the fitted temperature of 1800 K. A geometrical viewing factor correction was made to the data, multiplying the observed flux by 1.12 at $\theta = 0$, decreasing linearly to 1.00 at 53°.

For laser power adjusted so that the maximum surface temperature (T_{\max}) reached was about 1825 K, we obtained angular flux distributions for D_2 desorbing from W at varying D_2 exposures. These are shown in Fig. (6)

and fitted temperature versus angle are shown in Fig. (7). The H_2 data were found in all cases to be essentially the same as the D_2 data. At high initial coverages there is a striking angular variation of flux and temperature, the flux ratio between 60° and 0° being .05, about 1/10 that expected for a cosine distribution. The corresponding temperature ratio is .3. At low initial coverage the flux is much less peaked toward the normal and the temperatures are much more nearly constant. Figs. (8) and (9) show the temperatures and fluxes for high initial coverages but varying degree of laser heating. The flux was obtained somewhat differently than the rest of the data: the time integrated detector signal was recorded as a function of laser heating at both 0 and 60° from the normal. These numbers were then multiplied by the square root of the fitted temperatures interpolated from Fig. (8) to approximately correct for the velocity sensitivity of the detector. Clearly most of the D_2 desorbed for surface temperature maxima above 1750 K and very little desorbed for T_{\max} less than 600 K. At low T_{\max} the flux ratio is higher than at higher T_{\max} . The temperature behaviors in Fig. (8) are very different for 0 and 60°. As T_{\max} is changed from 500 to 3000 K the fitted temperature for $\theta = 60^\circ$ ranges from 540 to 630 K. For $\theta = 0$ the fitted temperature increases rapidly at first from 720 K, then more slowly up to 2100 K.

V. Discussion

At first it seemed that we had discovered non-cosine distributions similar to those observed for hydrogen on clean single crystal Cu (24) or on contaminated surfaces. (25, 26) Two observations of nonthermal, noncosine hydrogen evaporation from sulfur covered Ni have been made; (27, 28) the latter work shows angular variations of flux and energy qualitatively very similar to our data at high coverage, full desorption. Model calculations of hydrogen recombination on W (100) by McCreery and Walken (28) show a marked preference for desorption toward the normal for both atoms and molecules (however, H atoms desorbing from polycrystalline W have been observed to show cosine behavior (18)). Despite these precedents, we believe that our unusual data is an artifact of gas-phase collisions between the desorbing molecules. We tested this by using a much longer laser pulse (700 microseconds) to desorb completely a high coverage layer of D₂. This reduced the number density of desorbed molecules near the surface. Under these conditions we obtained a nearly cosine flux distribution. Furthermore, the data approach a thermal cosine behavior as the amount desorbed decreases, either by fully desorbing decreasing initial coverages, or by desorbing less and less of a high initial coverage. This is demonstrated in Fig. (10) where the ratio of fitted temperatures is plotted versus the ratio of desorbed flux between 60° and 0° from the normal, the data taken from Figs. (6-9). The two data sets have clearly the same trend as the amount desorbed decreases. This

behavior would be expected for a collision process, and contradicts most alternative explanations of the data based on differing adsorption sites or desorption mechanisms at high or low initial coverages. Finally, the following estimation of the collision probabilities supports this hypothesis.

Collision Effects

The effect on our data of collisions between molecules after they leave the surface depends on the fraction which experience collisions, and then only to the extent that the collisions modify the angular flux and velocity distributions. Although detailed calculations of collision effects would be difficult, analysis of a simple model shows the qualitative nature of the effects and gives reasonably quantitative estimates of the collision probabilities. We will show that the flux and velocity distributions are altered by two different but reinforcing effects: (1) a "kinetic" effect involving the dependence of collision probability with the initial speed and angle of departure of the molecule from the surface. This causes a selective depletion by collision of slower molecules traveling at small angles to the surface normal, and depletion of the faster ones at large angles; (2) a "kinematic" effect on the redirection of molecules after collision due to the restrictions of conservation of energy and momentum.

In this experiment, the length of time over which significant desorption occurs is about 10^{-8} sec. ■ τ . This is very much smaller than the time

required for a typical molecule to travel a distance comparable to the diameter ($2R$) of the laser irradiated surface. By the time the molecules have traveled R , the density has dropped to a value very much smaller than existed earlier, and collisions beyond this point contribute negligibly to the total. This implies that during the time significant collisions occur the surface acts like an infinite plane, simplifying the analysis. The desorption/expansion can be further divided into two stages. Stage 1 is limited in time from $t = 0$ to τ , during the actual desorption. In stage 1 the velocity distribution of molecules resembles that of a bulk gas (except v_z , the normal velocity component of a molecule, must be > 0). We assume for our model that the gas desorbs Maxwell-Boltzmann-like, isothermally, and uniformly over time τ . Stage 2 is limited by $\tau < t < R/|v|$, i.e., after the actual desorption but before radial thinning (v is the velocity of a particular molecule). During stage 2 velocity segregation develops, that is, molecules with larger normal components of velocity tend to be found farther from the surface than slower ones. As t becomes $\gg \tau$, molecules with a particular v_z will be found only near $z = v_z t$. For isothermal desorption of N molecules/cm² over time τ , the number density as a function of $z = v_z t$ and t , for $t \gg \tau$, can readily be shown to be:

$$n(v_z t) = (2N/\alpha)(v_z/\alpha) \exp(-(\nu_z/\alpha)^2) \quad (5)$$

with $\alpha = (2kT/m)^{1/2}$. This is plotted in Fig. (11). We see that in stage 2 the number density in the vicinity of a particle depends strongly on its

normal velocity component, whereas in stage 1, no such systematic dependence is expected. Also, this $n(v_z = z/t, t)$ has a maximum value at any particular time at $v_z = \alpha/\sqrt{t}$. This is very different than a bulk gas, and results directly from the finite desorption time and the $|v| \cos \theta = v_z$ weighting of the desorption flux.

The total number of collisions a molecule experiences between times t_a and t_b , in the limit of low collision probability, is

$$\int_{t_a}^{t_b} dt \sigma_c n(t) g(v_z t),$$

where σ_c is the collision cross-section, here assumed constant, v_z and v are the position and velocity of this molecule, and $g(v_z t)$ is the average relative speed of this molecule with respect to the other molecules at t . In stage 2 this integral is strongly influenced by the density term. A particle which travels at angle θ from the surface normal will have a maximum collision probability near $v = \alpha/\sqrt{a}/\cos \theta$ giving a value of v_z for which the molecule travels continuously within the densest part of the wave of desorbed gas. Fig. (11) shows the value of this integral for stages 1 and 2 together, as calculated below, as a function of v for $\theta = 0$ and $\theta = 60^\circ$. Also shown is the total desorbed flux as a function of v . The peak collision probability is on the low velocity side of the flux distribution for $\theta = 0$, and on the high side for $\theta = 60^\circ$. This selectively depletes slow particles from the distribution at small angles and fast ones at large angles, and constitutes the "kinetic" altering of the velocity distributions.

The changes in velocity and direction of two colliding molecules are kinematically restricted, relative velocity and center of mass motion being conserved (presuming negligible transfer of energy to internal modes). For hard-sphere-like collisions this leads to a strong tendency for the directions of velocity of the two particles to each lie closer to the center-of-mass velocity after the collision than they were before. When, as in our case, the gas source is a surface, the center-of-mass velocity has the highest probability of pointing along the surface normal. This causes a net effect where particles involved in collisions are preferentially redistributed toward the surface normal.

Additionally, when one particle is scattered to larger angles from the center-of-mass velocity than either was originally, the one at large angle is likely to be slower, and the other faster, than either was before the collision. This contributes to an average speed which decreases with increasing angle. Still another kinetic effect is distinguishable particularly for "small angle" scattering, including the important soft potential and quantum diffraction part. For any group of particles with the same v_z , those with larger θ are necessarily faster. A net transfer of energy from those at large θ to those at small results from small angle scattering.

Assembling the above discussion into a numerical prediction proceeds as follows: During stage 1 the number of collisions/molecule should not depend strongly on velocity, and for a typical particle leaving at $t = \frac{1}{2} \tau$, ought to be roughly $\int_{v_0}^{\tau} dt \sigma_c (N/\tau/a) a = \frac{1}{2} N \sigma_c$. For stage 2, if we

use the v_z stratified particle density approximation (Eq. 5) from $t = \tau$ to R/v , the number of collisions/molecule is

$$2N\sigma_c (\ln(R/\tau/a) + h(a/v)) v \cos \theta / a \exp(-v(\cos \theta/a)^2) ((v \sin \theta/a)^2 + \pi/a)^{\frac{1}{2}} \quad (6)$$

The last term is a convenient approximation for the average relative velocity, good to 5%. These expressions are independent of T and τ for v in units of a , except for a weak logarithmic dependence on $R/\tau/a$, thus supporting the notion that the two data sets of Fig. (10) should be comparable as presented. The absolute importance of collisions is fixed primarily by $N\sigma_c$. Parameters corresponding to the data presented for full desorption of a high coverage layer of deuterium are $N \approx 3.8 \times 10^{14}$ molecules/cm², $\sigma_c \approx$ van der Waals collision cross-section $\approx 1.8 \times 10^{-15}$ cm², $R = .1$ cm, $T = 1290^\circ K$ (our own estimate), $a = 2.3 \times 10^5$ cm/sec. For $\theta = 0$ the maximum collisions / molecule is $.3 + 2.1 = 2.4$ (stage 1 + stage 2), for $\theta = 60^\circ$ it is $.3 + 2.9 = 3.2$. This is the scale used in Fig. (11). Obviously 3.2 is not much less than 1, invalidating the perturbational approach used, but the importance of collisions is demonstrated. For the lowest initial coverage data reported, the maximum collisions / molecule is calculated to be $.2$ to $.3$. This is small compared to 1, and indeed the angular flux and velocity distributions appear only moderately different from thermal $\cos \theta$.

In view of the qualitative agreement between the calculated effects of collisions and our data, the data of Fig. (10), and the near $\cos\theta$ desorption found at very much slower heating rates, it seems likely that collisions between molecules after they leave the surface are responsible for our apparent non-thermal non cosine data.

Collisions will not be important if $N\sigma_c \ll 1$. Full monolayers usually have $N\sigma_c \lesssim 1$, 1 being nearly an absolute upper limit. This is because the area occupied / molecule = V/N , and $1/N_{\max} \approx \sigma_c$ because of intermolecular repulsions. Collisions will not be important even for $N\sigma_c \approx 1$ if $T \gg R/a$, that is, if radial thinning occurs while the desorption is still proceeding.

Desorption Kinetics

Collisions complicate the comparison of our results with our expectations for the variation of flux and velocity distributions with laser induced surface temperature and initial coverage, or with kinetic data obtained by conventional means. Despite redirection of desorbed flux, the total amount desorbed should be conserved. In addition, to the extent that the collisions are elastic, that is, no significant transfer of translational energy into internal modes occurs, an angular average of the energy should be free of collision effects. The flux weighted, angularly averaged temperatures (\bar{T}_s) for varying D_2 exposures at constant maximum surface temperature were calculated from the interpolations of Figs. (6) and (7), and appear in Table 2. At varying maximum surface temperature, data were only taken at 0 and 60° , preventing direct angular averaging. It is a reasonable supposition that because of the simple kinematics of collisions the following relations for \bar{T} and the angularly averaged flux, \bar{F} , might approximately hold

$$\bar{T} = T_0 \cdot a(T_0 / T_{60}) \quad \bar{F} = F_0 \cdot b(T_0 / T_{60}) \quad (7)$$

where T and T_{60} are the fitted temperatures at 0° and 60° from the normal, and a and b are functions only of the temperature "peaking ratio." We have interpolated a and b from the data at varying D_2 exposure and used it to estimate \bar{T} and \bar{F} for the data at varying laser heating. The results appear in

Figs. (8) and (9). In view of the correlation between the two sets of data shown in Fig. (10), it is reasonable to estimate \bar{T} and \bar{F} in this way.

\bar{T} from Table II at low initial coverage should correspond to the isothermal limit of desorption. With the help of a numerical simulation of the desorption, it served to accurately fix the relation between laser power and T_{\max} , the maximum surface temperature, as discussed before. The variation of \bar{F} with T_{\max} is roughly as expected—a sharp threshold at low T_{\max} , and \bar{F} leveling off at high T_{\max} where near complete desorption occurs. At low T_{\max} , \bar{T} is near but somewhat above the line $\bar{T} = T_{\max}$ expected for the isothermal limit (Fig. (8)). This sort of deviation would be produced by inhomogeneous laser heating. The temperature calibration was done at low initial coverage. A section of the surface which received less light than the average and had an appropriately smaller local T_{\max} would desorb less than the average if all started at the same initial coverage. But because the data were collected during sequential adsorptions / laser desorptions, the initial coverages after ≈ 2 desorptions were locally higher or lower than the average such that the amount desorbed per unit area was relatively independent of local variations in laser irradiance. Thus the laser calibration obtained at low initial coverage reflects the average T_{\max} reached. At near monolayer coverage in the isothermal limit, the initial surface coverage has little ability to adjust for local variation in laser irradiance so the regions with higher than average laser irradiance dominate the desorbed flux. This is why

\bar{T} is higher than T_{\max} for low T_{\max} in Fig. (8).

A direct comparison of the \bar{T} 's in Fig. (8) and Table II, and \bar{F} in Fig. (9) was made with the result for numerical integration of the kinetic model of Hickmott (2) for H_2 on tungsten. His kinetic model has a preexponential of $2.5 \times 10^{-3} \text{ cm}^2/\text{atom}$ and an activation energy of about 31 Kcal/mole at 0 coverage, decreasing to 19 Kcal mole at $9 \times 10^{14} \text{ atom/cm}^2$. There is general agreement between our data and Hickmott's predictions. The deviations of \bar{F} at low laser power above that of Hickmott's curve is, again, expected for inhomogeneous laser irradiance.

Clearly, within the limitations of this preliminary experiment, the desorption of D_2 from polycrystalline W at rates of $5 \times 10^7 \text{ monolayers/sec}$ appears governed by the same kinetics as H_2 desorption at rates 10^5 or more times slower.

VI. Future Work

We are making improvements in our apparatus for future work. The laser will be modified to give better spatial uniformity for heating, and variable length pulses to increase the range of heating rates accessible. Collision effects can be dealt with in several ways. At highest heating rates for full monolayer desorption, angular averaging is perhaps the only recourse, and will only work if the collisions conserve translational energy. Desorption of much less than a monolayer greatly reduces collisions. If the desorption time is increased toward several microseconds, the density of

described molecule will be low enough to greatly reduce collisions, while still providing adequate time resolution for velocity distribution analysis.

TABLE I
Calculated D₂ Coverages

<u>Acknowledgement</u>	<u>D₂ Pressure</u>	<u>Exposure after 20 seconds</u>	<u>σ after one exposure</u>	<u>σ after repeated exposure/desorption</u>
Research sponsored by the Air Force Office of Scientific Research, Air Force Systems Command, USAF, under Grant No. AFOSR-77-3186, and by the Office of Naval Research.	7.5×10^{-8} †	$1.1 \frac{\sigma_{\max}}{\Sigma_0}$ (assumed)	$0.80 \sigma_{\max}$	$0.82 \sigma_{\max}$
We are grateful to the University of Chicago Central Development Shop, and particularly to the late A. Dudiak, for an outstanding job in fabricating the main apparatus.	7.5×10^{-9}	0.11	0.11	0.12
	2.5×10^{-9}	0.037	0.037	0.04 - 0.05 *

*depending on desorption model used

FIGURE CAPTIONS

TABLE II
Angularly Averaged Temperatures for Varying D_2 Exposures,
and Comparison with Predictions from Hickmott's Kinetics

D_2 Pressure (20 second exposure)	T_{\max}	$\bar{T}_{\text{expt.}}$	\bar{T} from Hickmott
7.5×10^{-8} torr	1830 K	1288 K	1316 K
7.5×10^{-9}	1830	1608	1657
2.5×10^{-9}	1790	1700	[1700] (used to calibrate laser heating)

Fig. 1 Calculated W surface temperatures for laser heating.

Assumed incident laser power is also shown.

Fig. 2 E and $\Delta T_{\frac{1}{2}}$ plotted versus t_p calculated by numerical integration of first order desorption kinetics with $v_1 = 10^{13} / \text{sec}$, at various linear heating rates as indicated. The E versus T_p curves originate at the lower left, the $\Delta T_{\frac{1}{2}}$ versus T_p curves from the upper left.

Same as Fig. (2), but for second order kinetics with $v_2 \sigma_0 = (10^{-3} \text{ cm}^2 / \text{sec}) (10^{15} / \text{cm}^2)$.

Fig. 3 Sample data showing mass spectrometer current (at mass 4) for a strong and weak signal case; the angle θ from the surface normal is indicated. Data were collected into a 200-2 μsec channel signal averager. No subtraction of background has been made.

Fig. 4 Experimental velocity distributions (discrete points) for desorbed D_2 and best fitted Boltzmann distributions (solid curves) at $\theta = 0$ (a, c) and $\theta = 60^\circ$ (b, d) from the normal. D_2 exposure for 20 seconds at 7.5×10^{-8} torr for a), b), and at 2.5×10^{-9} torr for c), d). Fitted temperatures are a) 1885K; b) 603K; c) 1985 K; d) 1633 K. Data points are bunched toward lower velocities to keep the point density manageable.

Fig. 6 Angular D_2 flux measured for nearly full desorption after exposures to D_2 at pressures indicated for 20 sec. Maximum surface temperature reached is about 1830 K for the two higher pressure curves and 1790 K for the lowest pressure curve. A cosine θ curve is shown for comparison.

Fig. 7 Fitted Boltzmann temperatures versus observation angle for nearly full desorption at various D_2 pressures indicated, for same data as Figure (6).

Fig. 8 Fitted Boltzmann temperatures versus maximum surface temperature for desorbed D_2 at $\theta = 0$ and 60° . D_2 pressure was 7.5×10^{-8} torr, for 20 second exposures. \bar{T} is the angularly averaged temperature (see text). \bar{T} predicted by desorption simulation with Hickmott's kinetics is also shown.

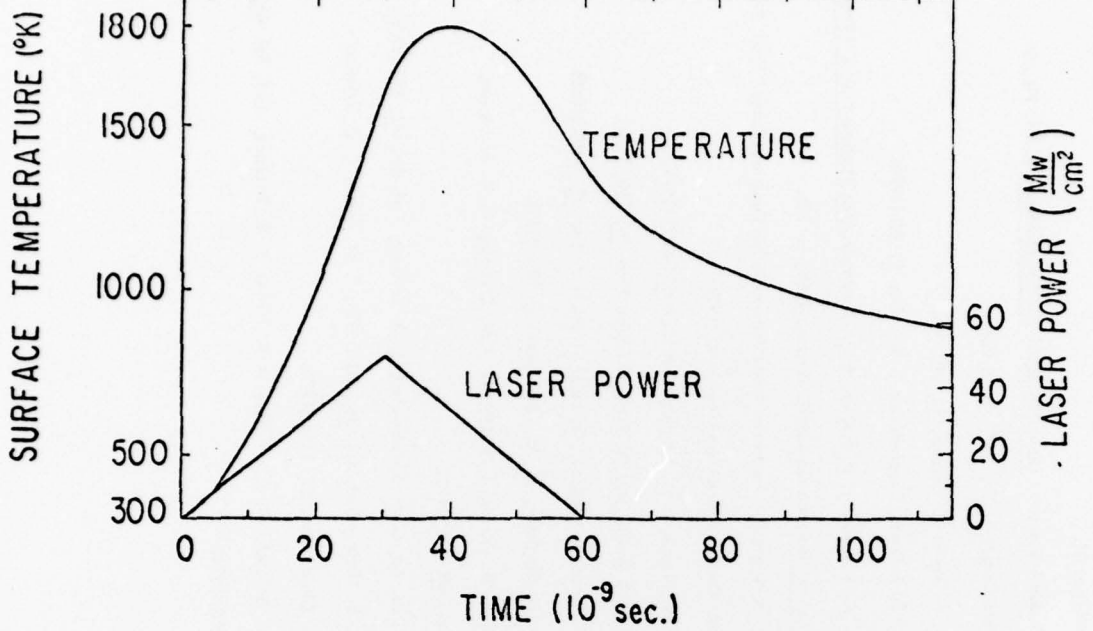
Fig. 9 Desorbed D_2 flux versus maximum surface temperature at 7.5×10^{-8} torr D_2 at 20 second exposures. Data at 0° and 60° is shown as well as the angularly averaged flux, \bar{F} (see text). \bar{F} predicted by Hickmott's kinetic data is also shown.

Fig. 10 Ratios of D_2 flux observed at 60° to that at 0° plotted versus the ratios of fitted D_2 temperature at 60° to that at 0° . Diamonds are for data at decreasing initial coverage (D_2 pressure = 7.5×10^{-8} , 7.5×10^{-9} , 2.5×10^{-9} torr) and maximum desorption temperature = 1830 K. Points with error bars are data at decreasing laser heating with D_2 pressure at 7.5×10^{-8} torr (all at 20 second D_2 exposure).

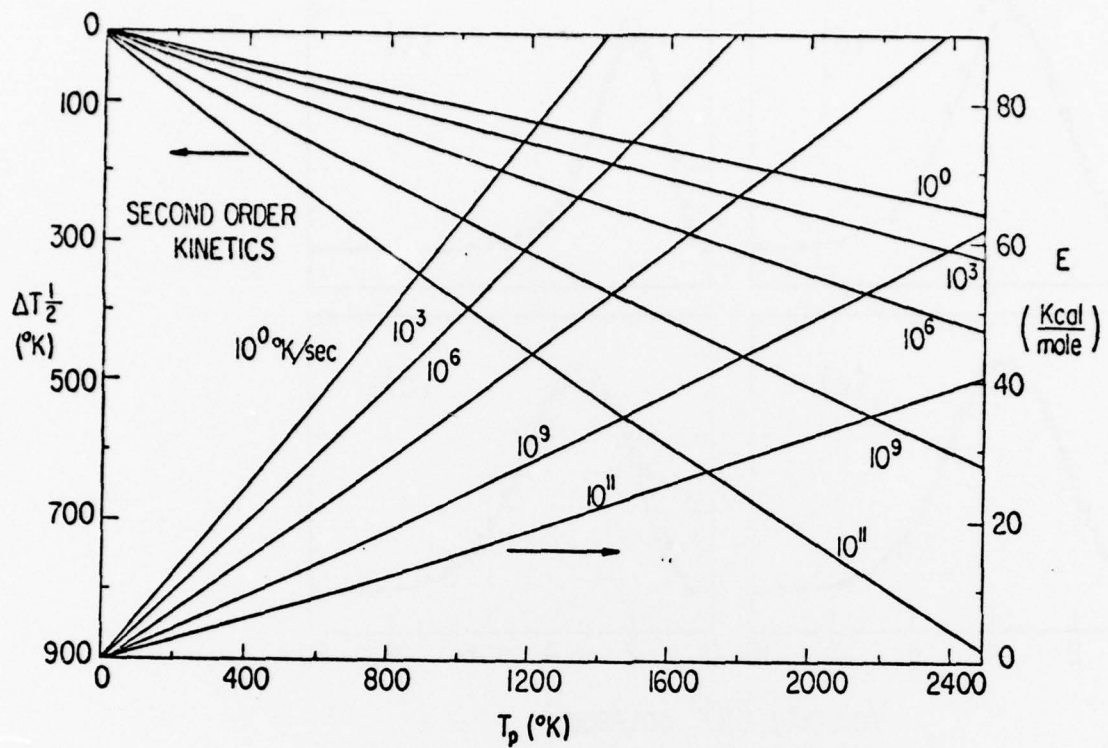
Fig. 11 Flux, number density, collision probability: Dashed curve is a Boltzmann distribution of flux vs. velocity. Dotted curve is the number density above the surface due to the desorbed gas during stage 2 (Eq. 5) plotted versus $v_z \sim z/t$. $\theta = 0$ and $\theta = 60^\circ$ curves are the number of collisions/particle estimated for particles travelling at $\theta = 0$ and $\theta = 60^\circ$ from the normal at velocity v for desorption of a monolayer of D_2 on W , calculated from Eq. (6).

REFERENCES

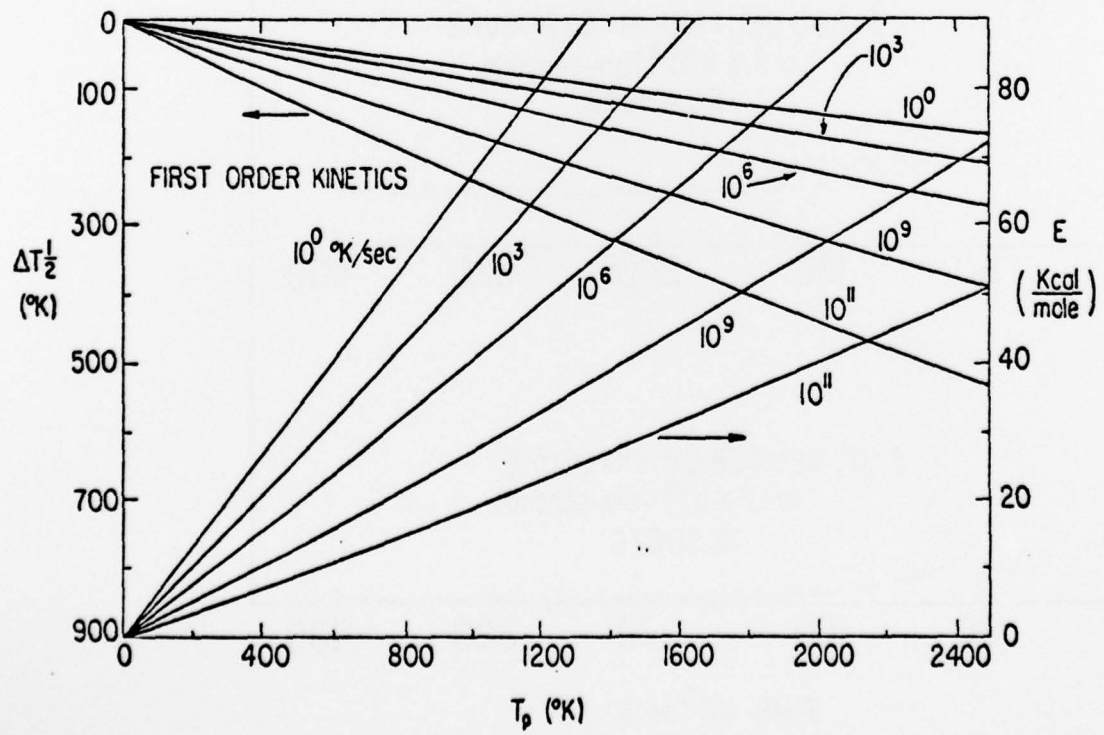
1. R. L. Palmer, Technical Report, Office of Naval Research, IRT 8162-001, Oct. 20, 1977.
2. T. W. Hickmott, J. Chem. Phys. 32, 810-23 (1960).
3. G. F. Ivanovskii, S. V. Vankov, Zavod. Lab. (Russ.), Pub. 69, series 35, issue 8, 959-61.
4. John F. Ready, Effects of High Power Laser Radiation (Academic Press, N.Y., N.Y. 1971).
5. N. G. Unterbeck, S. P. Tang, J. F. Friichtenicht, Physics of Fluids 12, 900 (1975); R. A. Olstad, D. R. Olander, J. Appl. Phys. 46, 1499 (1975).
6. S. M. Bedair, Harold P. Smith, Jr., J. Appl. Phys. 40, 4776 (1969)
7. G. Ertl, M. Neuman, Z. Naturforsch. 27A, 1607 (1972); K. Christmann, O. Shabes, G. Ertl, M. Neumann, J. Chem. Phys. 60, 4528 (1974); L. P. Levine, J. F. Ready, E. Bernat, J. Appl. Phys. 38, 331 (1967); B. V. Bondarenko, V. A. Kurzetsou, A. A. Shechuka, Sov. Phys. Tech. Phys. 18 (a), 1255 (1974); J. M. Chen, C. C. Chong, J. Appl. Phys. 43 (a) 3884 (1972).
8. R. Smoluchowski, Phys. Rev. Lett. 35, 1385 (1975); S. Baidyary, W. R. Bottens, P. Mark, Surf. Sci., 28, 517 (1972).
9. N. F. Mott and H. Jones, The Theory and Properties of Metals and Alloys (Dover Publications, Inc., N.Y., N.Y. 1958).
10. D. E. Gray, ed., American Institute of Physics Handbook (McGraw Hill, N.Y., N.Y. 1957).
11. J. A. Stratton, Electromagnetic Theory (McGraw Hill, N.Y., N.Y., 1941) p. 31.
12. Purdue University, Thermophysical Properties of Matter (I. F. I. Plenum Data Corp., N.Y., N.Y. 1970) Vol. 1.
13. P. A. Redhead, Vacuum, 12, 203 (1962).
14. L. D. Schmidt, Catalysis Rev. - Sci. Eng. 2, 115 (1974).
15. P. A. Redhead, J. P. Hobson, E. V. Kornelson, The Physical Basis of Ultrahigh Vacuum (Chapman and Hall, London, 1968), p. 275.
16. E. S. Dayhoff, "Transverse Mode Patterns in Nd Glass and Ruby," Proc. 3rd Int. Congr. of Quantum Electronics (1962).
17. P. W. Tamm, L. D. Schmidt, Surf. Sci. 55, 4253 (1971).
18. Joe N. Smith, Jr., W. Fite, J. Chem. Phys. 37, 898 (1962).
19. F. Ricca, R. Medina, G. Saini, Trans. Far. Soc. 62, 1492 (1965).
20. J. H. Singleton, J. Vac. Sci. Tech. 5, 109 (1968).
21. R. P. H. Gasser, T. N. Morton, J. M. Overton, A. K. Szczepura, Surf. Sci. 28, 574 (1971).
22. S. M. Ko, C. H. Steinbruehl, L. D. Schmidt, Surf. Sci. 43, 521 (1974).
23. T. E. Madey, Surf. Sci. 36, 281 (1973); P. W. Tamm, L. D. Schmidt, J. Chem. Phys. 52, 1150 (1970).
24. M. Baloch, M. J. Cardillo, D. R. Miller, R. E. Stickney, Surf. Sci. 45, 358 (1974).



- 25. T. L. Bradley, A. E. Dabiri, R. E. Stickney, *Surf. Sci.* **29**, 590 (1972);
W. Van Willigan, *Phys. Lett. A* **28**, 80 (1968).
- 26. G. Comsq, R. David, K. D. Rendulic, *Int. Symposium on Molecular Beams*, Noordwijkerhout, Netherlands (1977).
- 27. A. E. Dabiri, T. J. Lee, R. E. Stickney, *Surf. Sci.* **26**, 522 (1971).
- 28. J. McCrae, G. Wolken, Jr., J. Chem. Phys. **64**, 2845 (1976).



F16.3



- 2

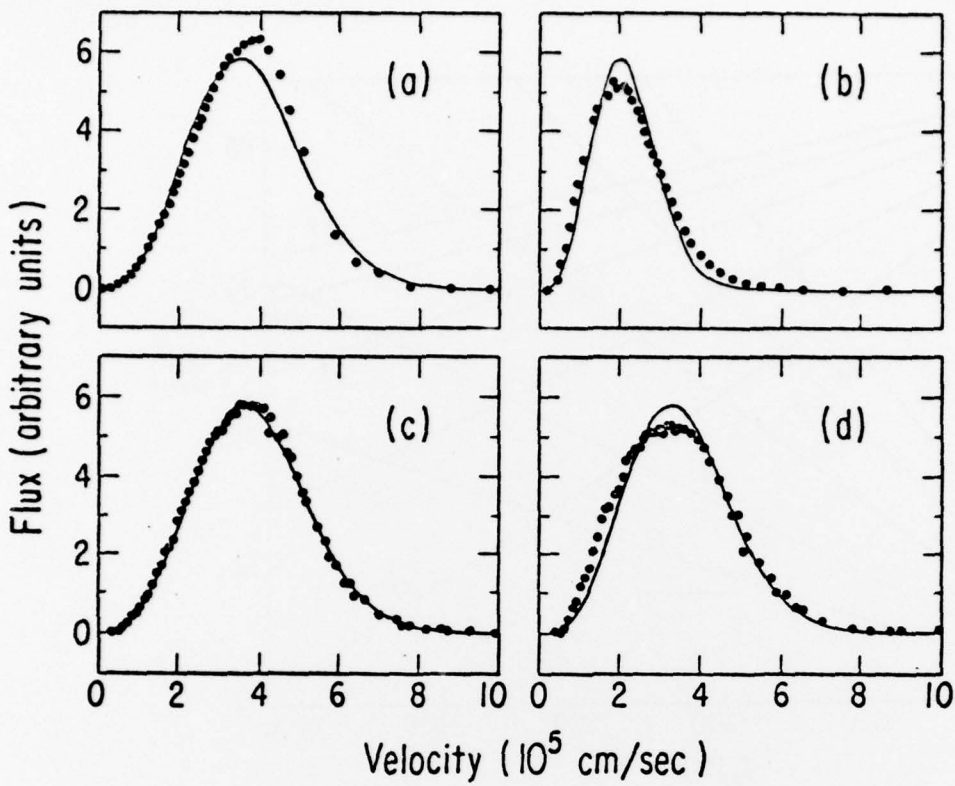
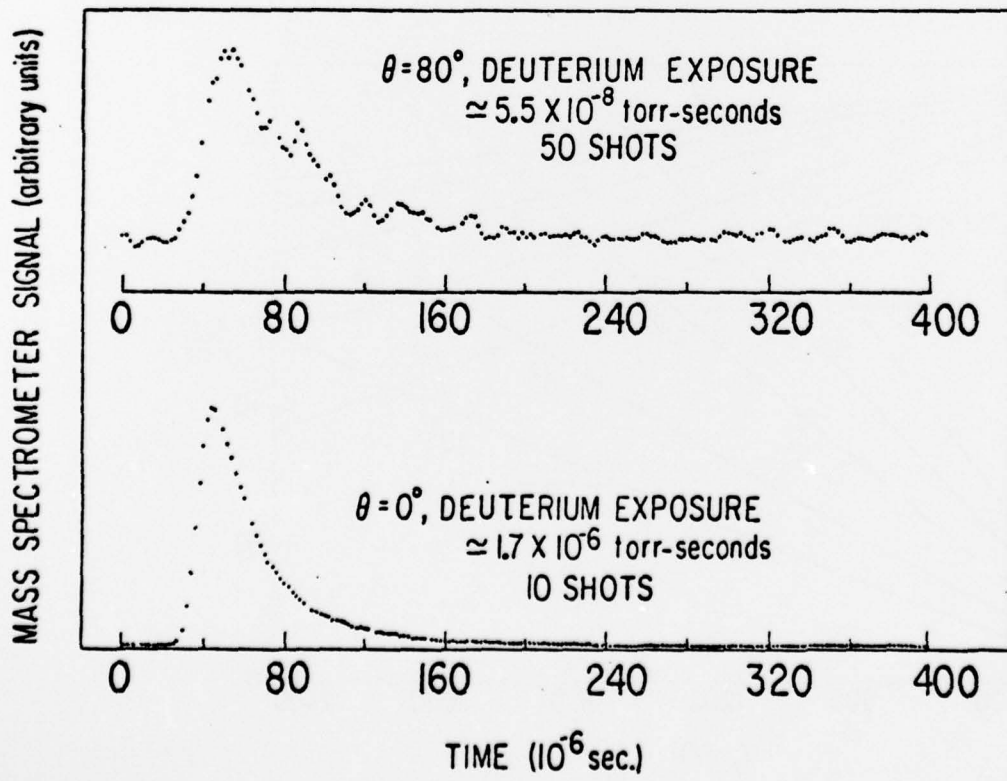


FIG 5



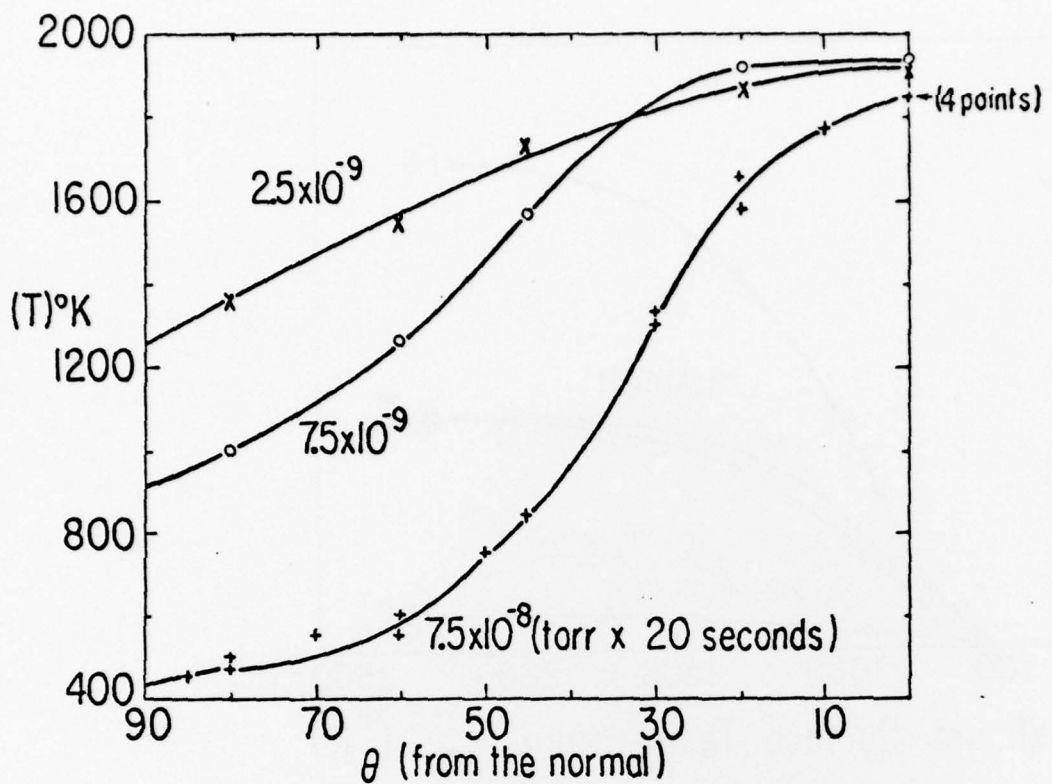
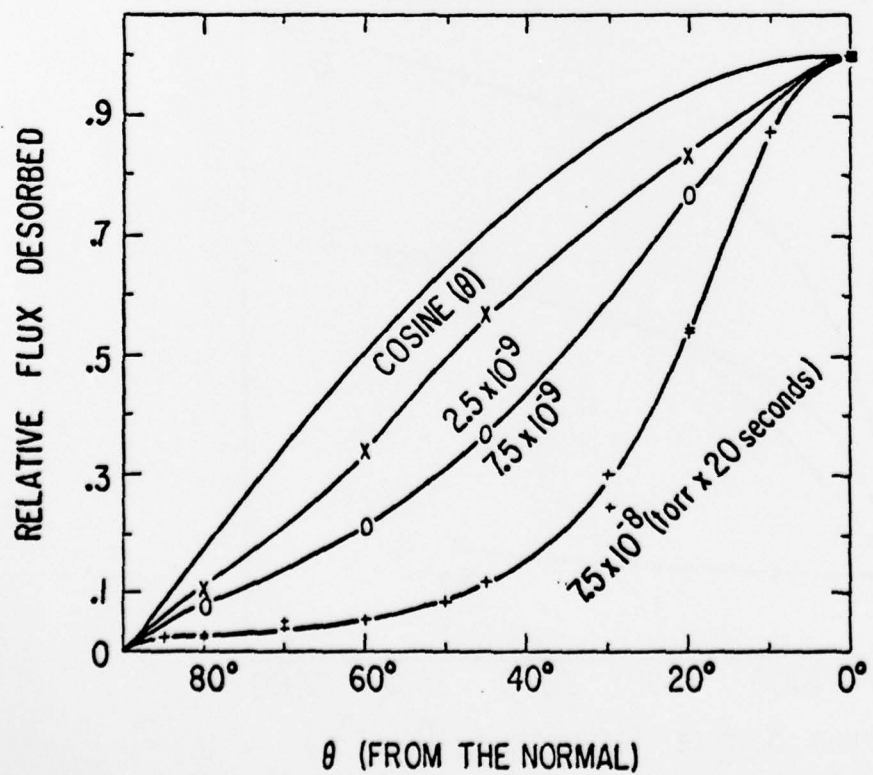


FIG 7



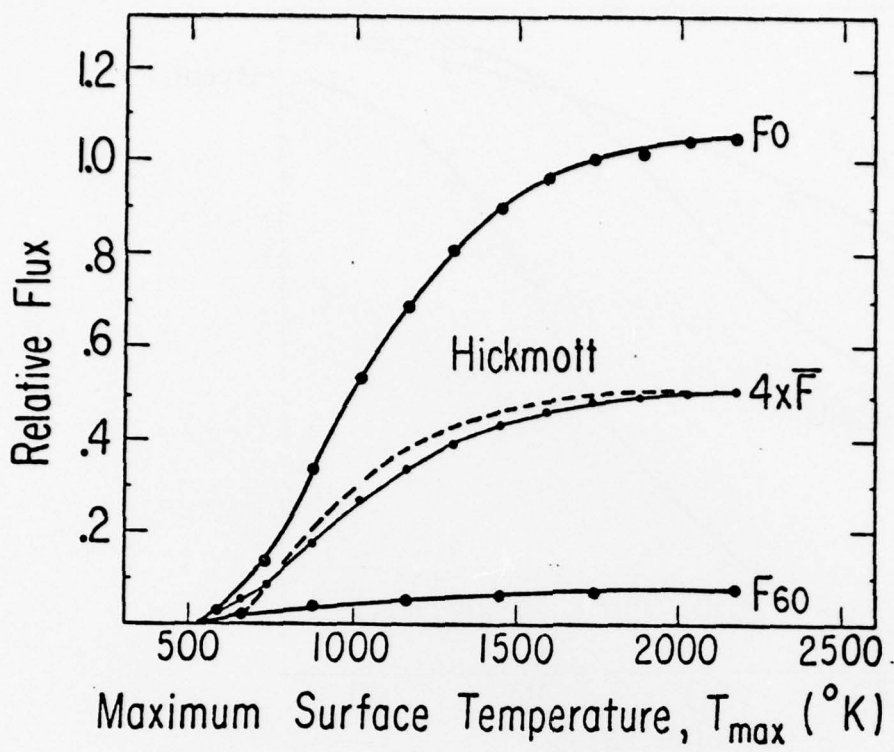


Fig 9

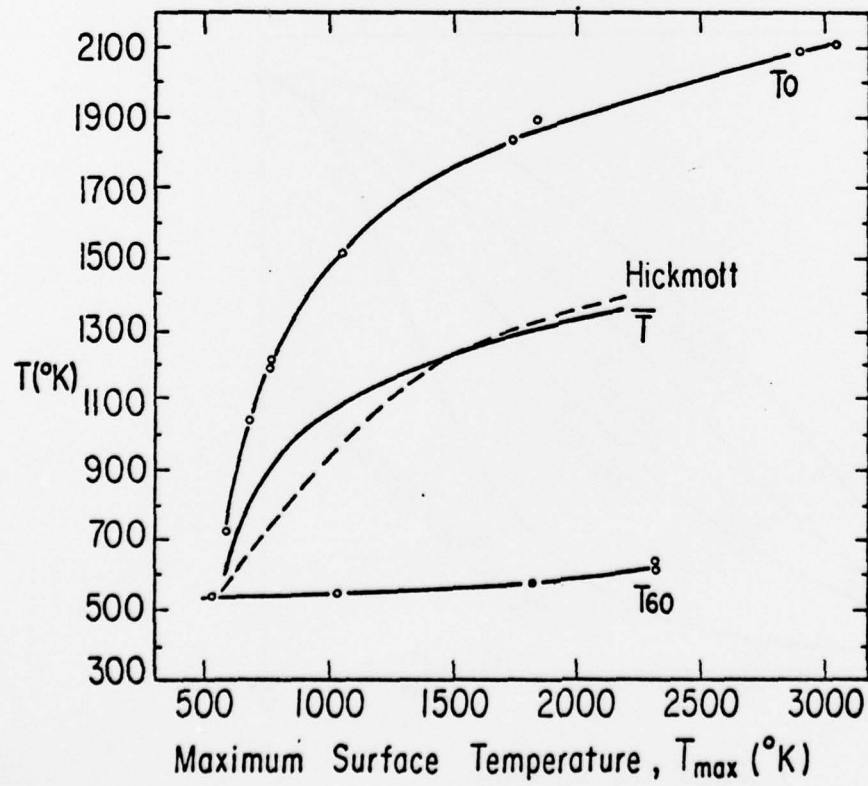


Fig 8

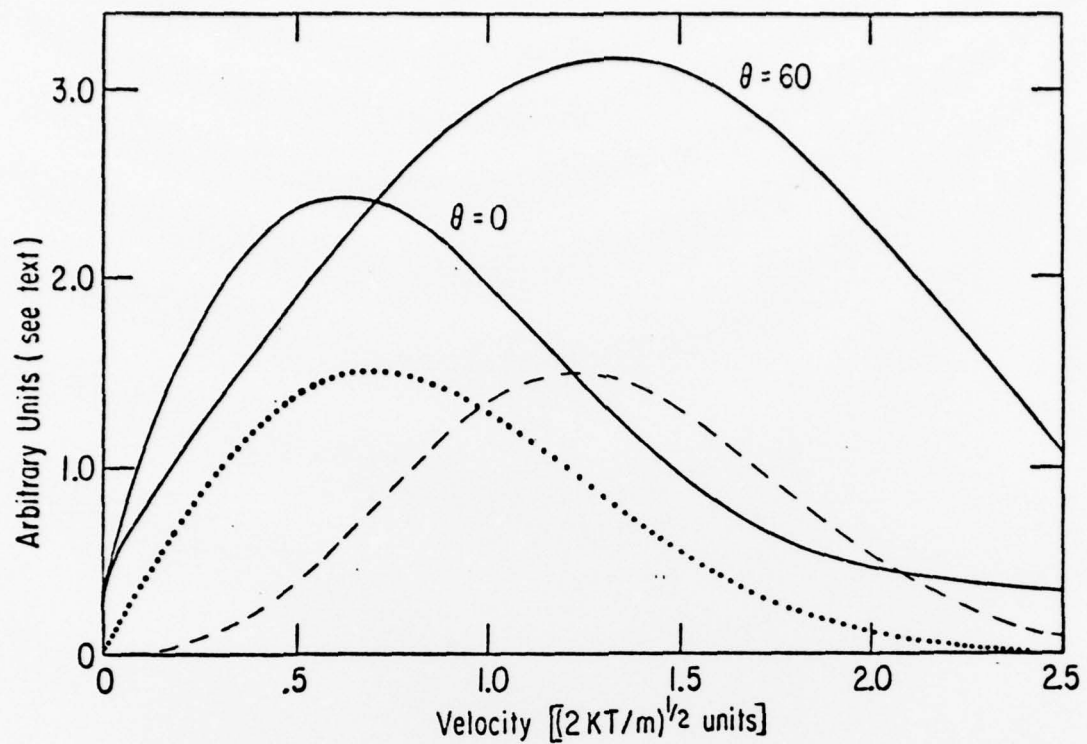
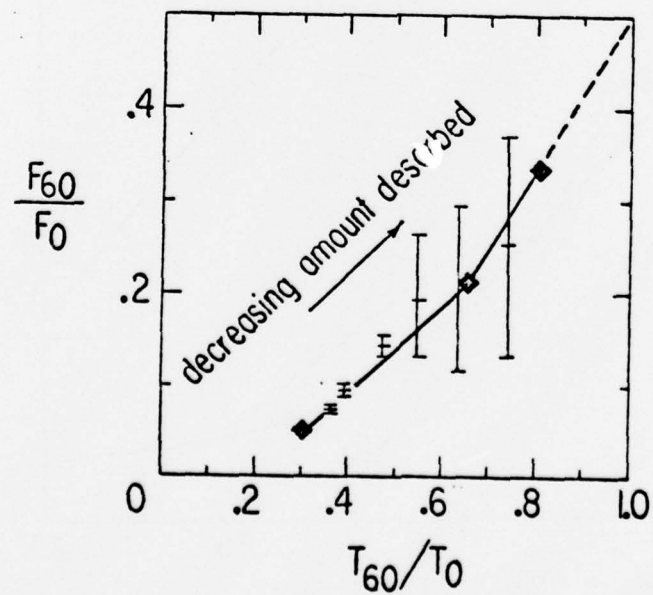
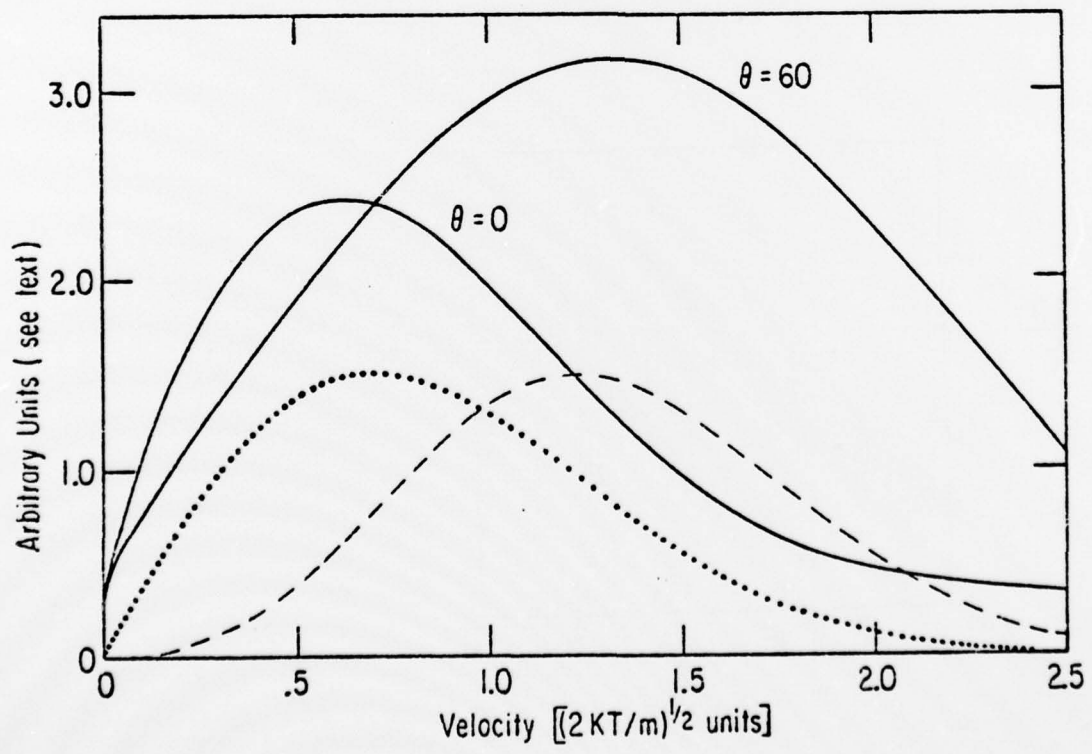


Fig 11





Fig"

